WELDING RESEARCH

SUPPLEMENT TO THE *WELDING JOURNAL*, OCTOBER 1992

Sponsored by the American Welding Society and the Welding Research Council

Diffusion Brazing in the Nickel-Boron System

Process variables are taken into account in developing a model for the four phases of diffusion brazing

BY J. E. RAMIREZ AND S. LIU

ABSTRACT. The principles of diffusion brazing were investigated using the nickel-boron system. Mathematical modeling of the process was carried out, followed by experimental verification of the model developed. The kinetics of melting and solidification in diffusion brazing was thoroughly characterized as a function of process variables such as temperature, time, interlayer thickness, filler metal composition, and the base metal composition. Boron diffusion in the base metal was the controlling mechanism during isothermal solidification of the liquid zone. The activation energy for boron diffusion in nickel between 1125° and 1225°C was estimated to be 39.7 kCal/mol. While liquid metal grain boundary penetration increased the kinetics of the solidification process, boron concentration change in nickel near to the interface decreased the chemical composition gradient and driving force for diffusion of boron into nickel. The results of this work can be used to assist in the development of interlayer materials for diffusion brazing of other more complex nickel alloy systems.

J. E. RAMIREZ and S. LIU are with the Center for Welding and Joining Research, Department of Metallurgical and Materials Engineering, Colorado School of Mines, Golden, Colo.

Paper presented at the AWS 71st Annual Meeting, held April 22–27, 1990, in Anaheim, Calif.

Diffusion Brazing

Diffusion brazing, also known as eutectic bonding, activated diffusion bonding, and transient liquid phase bonding, was first reported by Peaslee and Boam (Ref. 1) in 1952. The process combines the manufacturing ease of brazing with high joint strength, achievable only by solid-state diffusion bonding. The basic features of diffusion brazing are shown in Fig. 1. An interlayer of a specific composition and melting point is inserted between the parts to be brazed. The interlayer thickness is generally less than 250 μm (9.8×10^{-3} in.). The parts are held together under slight pressure, less than 1 atm (14.7 lb/in.^{2}), and heated to the brazing temperature in an inert atmosphere or vacuum (Ref. 2). Once the brazing temperature is reached, the interlayer may melt, or a liquid may form as the result of element diffusion between the interlayer and the base metal. The liquid, by capillary action, fills the joint clearance and eliminates potential voids at the interface between the two parts. While the parts are held at the brazing temperature, diffusion of alloying elements occurs between the liquid and the base metal leading eventually to isothermal solidification of the braze metal. Maintaining the brazed component at the brazing temperature after solidification will produce a joint with chemical composition and microstructure closely equivalent to those of the base metal.

KEY WORDS

Diffusion Brazing
Nickel-Boron System
Mathematical Model
Boron Diffusion
Isothermal Solidification
Pack Cementation
Process Variables
Reaction Kinetics
Chemical Composition
Activation Energy

Diffusion brazing has been described as a process comprised of four stages (Refs. 3, 4): 1) dissolution and melting of the interlayer; 2) homogenization and widening of the liquid layer; 3) isothermal solidification of the liquid zone; and 4) homogenization of the solidified bond region. Figures 2 and 3 show schematically the variation of composition in the joint region as the different stages of diffusion brazing take place.

Purpose of This Investigation

This research was conducted to study the controlling mechanisms and the re-

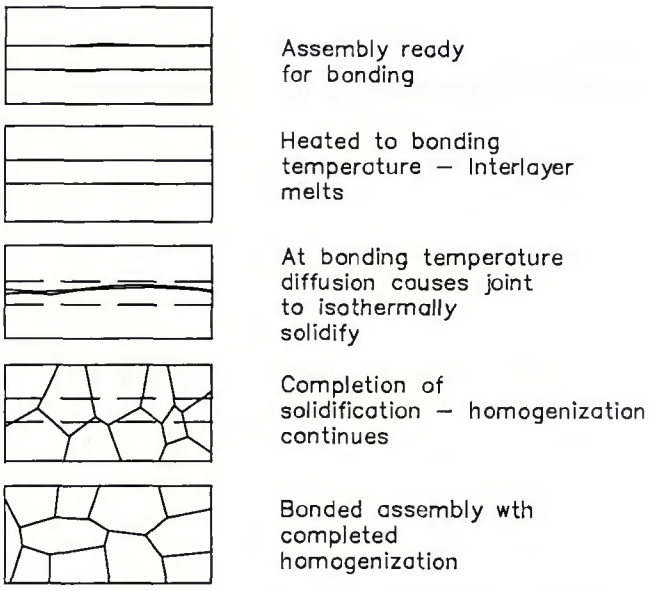

Fig. 1 — Functional description of the diffusion brazing process (Ref. 2).

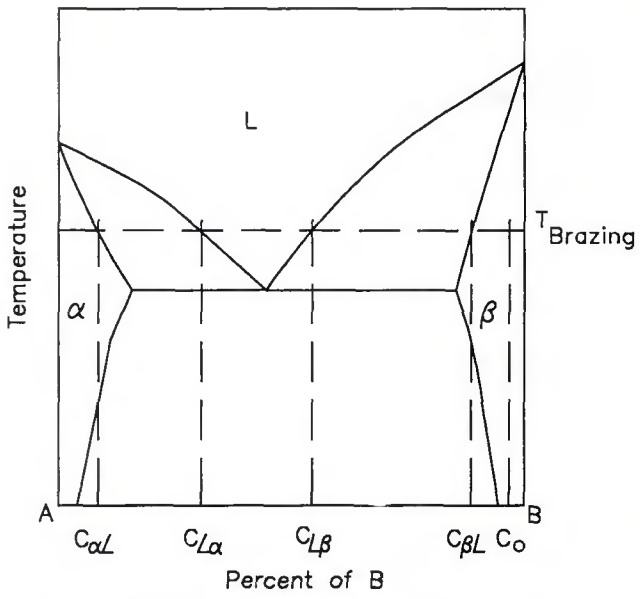

Fig. 2 — Typical binary equilibrium phase diagram with an eutectic reaction.

action kinetics of diffusion brazing. Nickel, being the base element of many superalloys, and boron, an element with high diffusivity, form the material system used in this study. The process was modeled mathematically and experiments were carried out to investigate the influence of temperature, interlayer thickness and composition, and the phase diagram of the alloy system on diffusion brazing.

Experimental Procedure

Nickel coupons of commercial purity (99.9 wt-%) were boronized in a graphite dish using the pack cementation process. The surfacing heat treatment was carried out in an electric furnace with argon atmosphere. Each nickel coupon was separated from the others by thin sheets of aluminum oxide and only the top surface of each specimen was exposed to the boron powder. Preliminary tests to determine the boronizing conditions were performed at 600°, 750°, 900° and 1000°C (1112°, 1382°, 1652° and 1832°F) for one, three and six hours. Metallographic analyses were done to characterize the thickness, uniformity and adherence of the surface layer. X-ray analyses were also used to identify the phases found in the boride coating.

Brazing of the boron-coated nickel specimens was carried out in a vacuum furnace at the temperatures of 1125°, 1175° and 1225°C (2057°, 2147° and 2237°F) and a vacuum of 1.33×10^{-6} kPa (1×10^{-5} torr). The specimens were held together under the pressure of a hand-tightened clamp for different periods of holding time (from minutes to hours), followed by cooling in the vacuum chamber. Aluminum oxide sheets were also inserted between the nickel specimens and the stainless steel clamp to prevent any contact reaction. The brazing thermal cycles are shown in Fig. 4.

Following the brazing experiments, the specimens were examined metallographically using Marble's reagent to determine the advance of the solid-liquid interface at a given time and temperature. The thickness of the remaining liquid layer in each sample was also determined, as an average of the measurements taken every 80 to 160 μm (3.1 to 6.2×10^{-3} in.) along the entire interface. The concentration profile of nickel across the bond region was determined using SEM-WDS (scanning electron microscope-wavelength dispersive spectroscopy). Attempts of direct determination of boron concentration with WDS were unsuccessful due to the low boron concentration (2 to 3 wt-%) in the bond region. The strong interaction of the boron characteristic x-ray radiation with the nickel matrix reduced drastically the intensity of the boron x-ray radiation and exhibited extremely high noise-to-signal ratio.

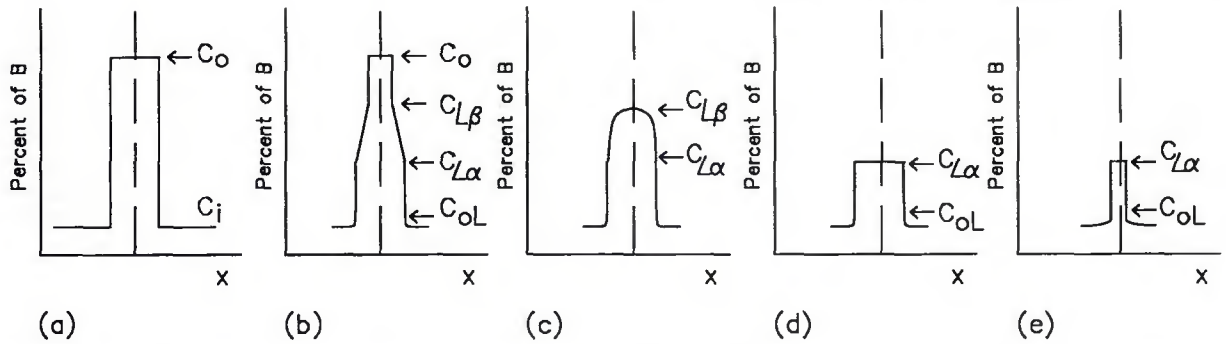

Fig. 3 — Schematic representation of the variation of composition with time in diffusion brazing. A–C — Dissolution of the interlayer; D — homogenization of the liquid region; E — isothermal solidification.

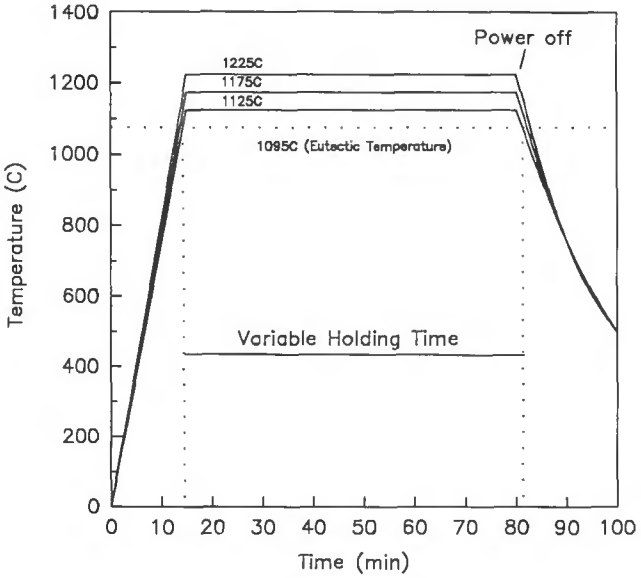

Fig. 4 — Schematic representation of the brazing thermal cycles.

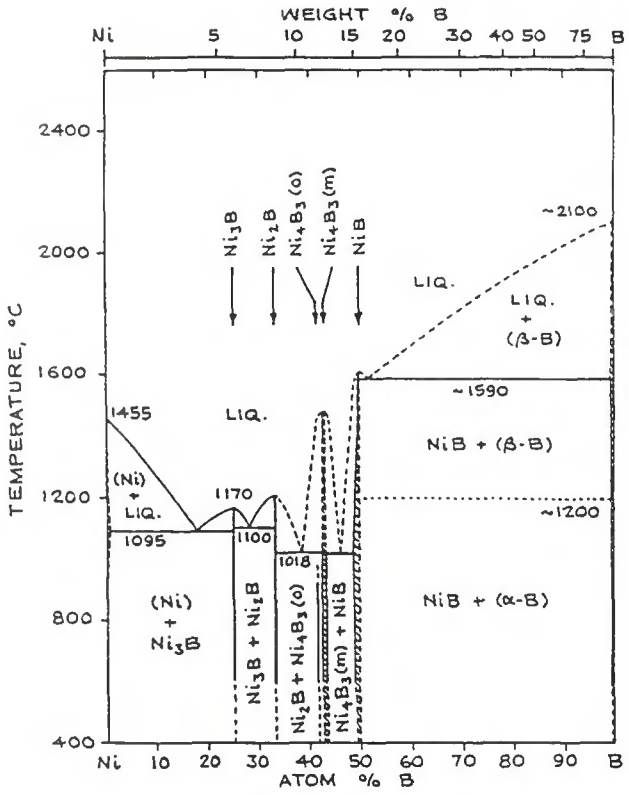

Fig. 5 — Nickel-boron equilibrium phase diagram (Ref. 6).

Results and Discussion

Boride Interlayer

The structure, thickness and phase composition of the boride coating prepared by diffusion saturation are strongly dependent of the composition of the saturation medium, the composition and structure of the material being boronized (Ref. 5), and the saturation temperature and time. As such, the phases encountered in the boride coating will be determined by the kinetic conditions such as rate of boron delivery to the surface and its diffusion rate into the metal, and by the stability of the different boride phases at the saturation temperature. The nickel-boron equilibrium phase diagram is shown in Fig. 5 to illustrate the many intermetallic compounds that may exist between nickel and boron.

X-ray analysis results showed that at temperatures below 900°C, no stable boride coating was formed on nickel. Above 1000°C, a thick layer of Ni_2B and Ni_3B formed rapidly. At 900°C, only Ni_3B was observed. Schoebel and Stadelmair (Ref. 7) indicated that Ni_2B was metastable at approximately 900°C and transformed readily into the more stable Ni_3B. Hence, all specimens were boronized at 900°C to have an interlayer with well-defined chemical composition and structure. Furthermore, Ni_3B and nickel form only a simple eutectic system, instead of the multiple eutectic reactions that may occur in case that a pure boron interlayer is paired with nickel in diffusion brazing.

The mean thickness of the boride layers was measured as a function of time and temperature of the chemical heat treatment process. The growth of the diffusion zone was found to obey the following equation:

$$X = Kt^n \qquad (1)$$

where X is the average thickness of the boride layer, K is a proportionality constant and characteristic of the transport mechanism, and t is the pack cementation time. The exponent n was determined to be 0.5, which suggests that the growth of the boride layer was controlled by volume diffusion of boron in nickel (Ref. 8).

Modeling of Diffusion Brazing

The development of the mathematical modeling of diffusion bonding has been presented by several authors (Refs. 9–11) and will not be detailed in this paper. However, the major results of the modeling work by Ramirez and Liu (Ref. 9) and experimental verification of their model are reported below.

Dissolution and Melting of the Interlayer

Considering an insert (or interlayer) of composition B positioned between parts of composition A, under equilibrium conditions, metal A will dissolve $C_{\alpha L}$ percent of B and metal B, $(100 - C_{L\beta})$ percent of A at temperature T_2 — Fig. 2. The solid solutions, α and β, will be in equilibrium with an intermediate liquid phase of composition that may vary from $C_{L\alpha}$ (in local equilibrium with α) to $C_{L\beta}$ (in equilibrium with β). The initial composition profile for this stage is indicated by Fig. 3A. After a small amount of diffusion has occurred, a narrow layer of liquid is formed on each side of the interlayer, producing a composition profile that is shown in Fig. 3B. The thicknesses of the two liquid regions, as shown in Fig. 3B, will increase while the thickness of the solid insert between them will decrease. At the moment that the solid interlayer is completely consumed, a single liquid zone of composition ranging from $C_{L\alpha}$ to $C_{L\beta}$, as shown in Fig. 3C, is formed.

In the case that boron is initially confined within a finite region, $-h < X < +h$, and considering unidimensional diffusion from a source of finite thickness, Ramirez and Liu (Ref. 9) proposed that the dissolution time (t_d) of an interlayer of thickness, 2h, at a given temperature

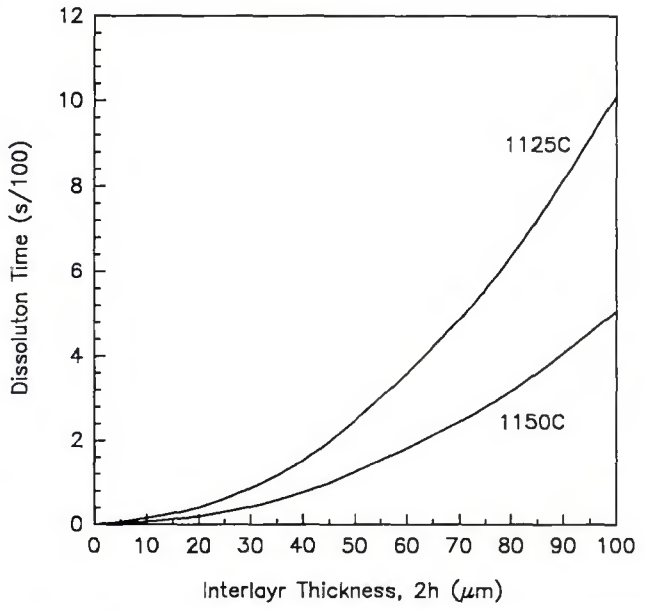

Fig. 6 — Dissolution time as a function of interlayer thickness, as predicted by the mathematical model for the Ni-Ni_3B system.

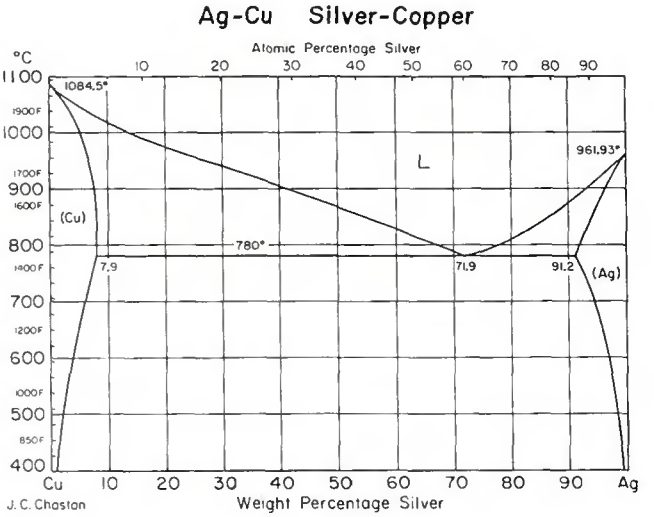

Fig. 7 — Silver-copper equilibrium phase diagram (Ref. 12).

could be determined by the following equation (Ref. 9):

$$t_d = \frac{(2h)^2}{16K^2 D_L} \quad (2)$$

where D_L is the liquid diffusivity of boron and K is a constant that depends on the alloy system. K can be obtained by solving the following equation (Ref. 9):

$$\frac{C_{L\beta}}{C_o} = erf(K) \quad (3)$$

C_o and $C_{L\beta}$ can be defined in the Ni-Ni_3B portion of the Ni-B equilibrium phase diagram.

At 1125° (2057°F) and 1150°C (2102°F), K was found to be 0.78 and 1.10, respectively. Due to the lack of reported data for boron diffusivity in liquid, the value of $D_L = 10^{-4}$ cm²/s (10^4 μm²/s) was assumed. As a result,

$$t_d = 1\times10^{-5}(2h)^2 \text{ at } 1125°C \quad (4)$$

$$t_d = 5.1\times10^{-6}(2h)^2 \text{ at } 1150°C \quad (5)$$

In these two equations, t_d is expressed in seconds, and 2h in micrometers. As can be seen in Fig. 6, the dissolution

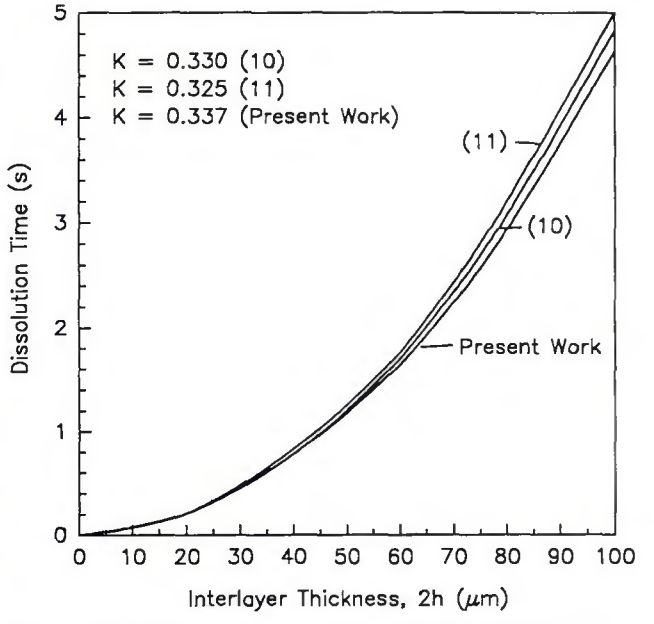

Fig. 8 — Dissolution time as a function of interlayer thickness, predicted by three mathematical models for the Ag-Cu alloy system at 820°C.

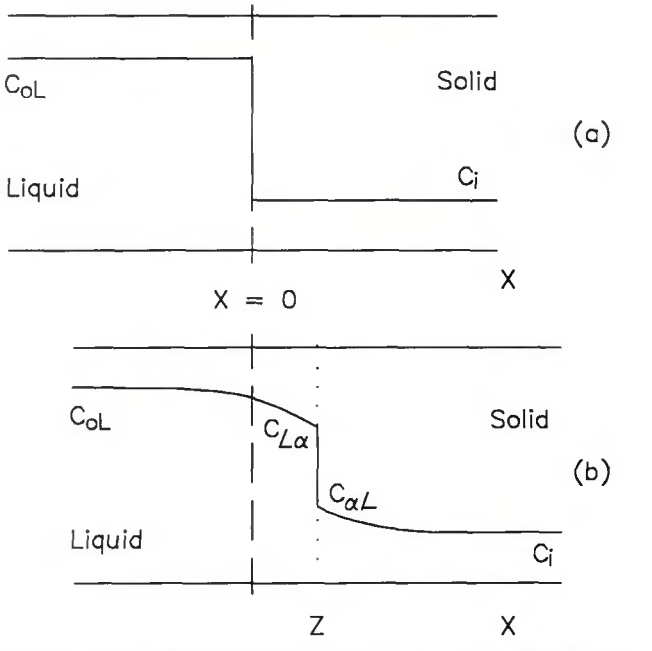

Fig. 9 — Homogenization of the liquid region. A — Initial conditions; B — boundary conditions at t > 0.

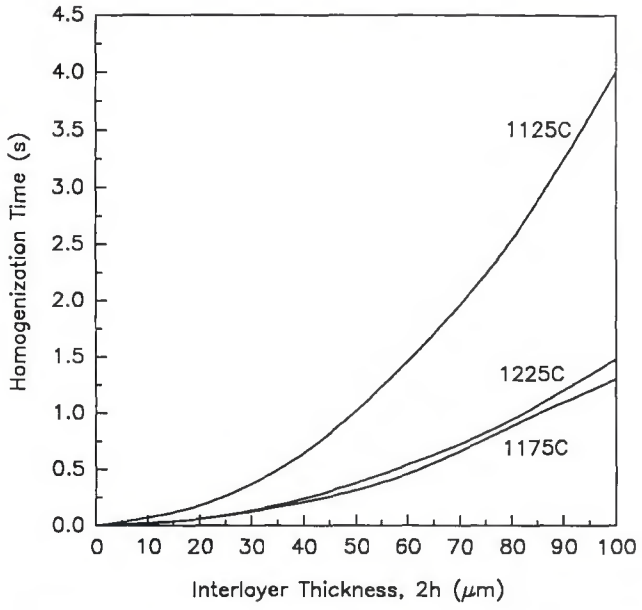

Fig. 10 — Homogenization time as a function of interlayer thickness, as predicted by the mathematical model for the Ni-Ni_3B system.

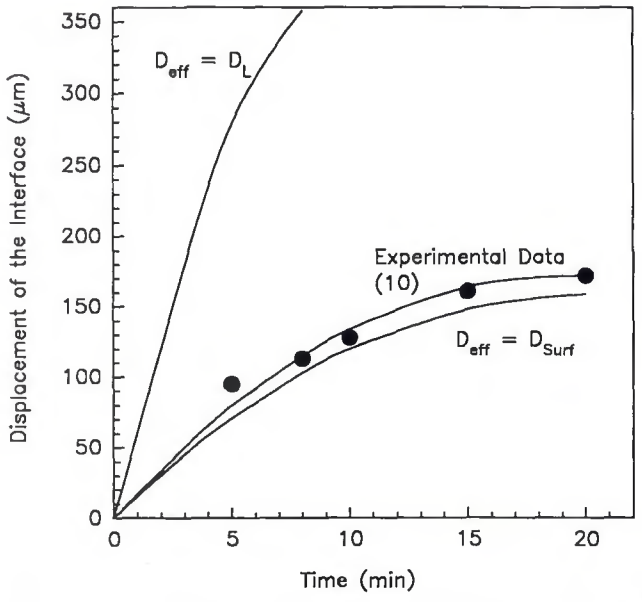

Fig. 11 — Displacement of the solid-liquid interface as a function of time, during homogenization of the liquid region, in the Ag-Cu alloy system.

time of an interlayer of thickness ranging from 0 to 100 μm (the range of practical applicability in diffusion brazing) required only fractions of a second. Thus, experimental observation of interlayer dissolution is very difficult and was not attempted in this work.

Comparable results have been reported in two other studies by Tuah-Poku, *et al.*, and Liu, *et al.* (Refs. 10, 11).

$$t_1 = \frac{(2h)^2}{16K_1^2 D_L} \quad (6)$$

$$t_1 = \frac{(2h)^2}{16K_2^2 D_L} \quad (7)$$

K_1 in Equation 6, proposed by Tuah-Poku, *et al.* (Ref. 10), can be evaluated from the solidus and liquidus compositions of the alloy system. These authors assumed an initially extended source of solute and a unidirectional displacement of the solid-liquid interfaces into the interlayer. Equation 7, on the other hand, considered active dissolution of both the interlayer and base metal, with the liquid region advancing into both the base metal and the interlayer (Ref. 11). In this equation, K_2 is a dimensionless growth constant related to the displacement of the interfaces. An initially extended source of solute was also assumed. Notice that the major differences between these two approaches and the approach taken in this work were the assumed initial distributions of the diffusing species and the movement of the solid interface. The different initial and boundary conditions led to different expressions for the evaluation of K in Equations 2 and 3. To determine the aptness of Equation 2 in predicting interlayer dissolution time, the equation was plotted together with Equations 6 and 7 using the Ag-Cu-Ag system for illustration. The K value was determined for 820°C using the Ag-Cu phase equilibrium diagram in Fig. 7. The time of interlayer dissolution and melting was calculated and plotted in Fig. 8. Note that Equation 2 predicts well the fast kinetics of the dissolution and melting of the interlayer during the diffusion brazing.

Taking into account that the "interlayer" used in this work (Ni_3B) was stoichiometric and that the nickel and boron diffusivities are greatly reduced due to the chemical bonding between these atoms. The accelerated kinetics observed during this first stage of diffusion brazing may be the result of high diffusion kinetics in the surface layers and interfaces (Ref. 13). Small amounts of nonstoichiometric Ni_3B may also be present and affect boron diffusion toward the base metal. The formation of a liquid film also accelerates greatly the diffusion process (Ref. 14).

Homogenization and Widening of the Liquid Region

When the liquid layer is in contact with the adjacent base metal, further diffusion of alloying elements takes place. The elements present in the liquid phase diffuse into the solid base metal while elements from the base metal migrate into the liquid phase, leading to the homogenization of the liquid region and further melting of the base metal. Finally, a wider liquid region of uniform composition $C_{L\alpha}$ results — Fig. 3D.

The net transfer of elements from solid to liquid, or vice versa, will depend on the relative amount and composition of the solid and liquid. The rate of mass transfer, however, is a function of the concentration gradients of the alloying elements in the system (Ref. 15). The isothermal mass transfer from solid to liquid in a concentration gradient can generally be considered to occur in two sequential steps. First, a surface reaction

Table 1— Composition Data and γh Parameter in the Ni-Ni_3B System

T(C)	C_{oL}(at.-%)	$C_{L\alpha}$(at.-%)	$C_{o\alpha}$(at.-%)	Ci(at.-%)	ϕ	C_o(at.-%)	γh
1125	17.0	14.5	0.18	0	227.7	25.0	0.091
1175	18.8	12.7	0.16	0	27.7	25.0	0.212
1225	17.7	10.4	0.12	0	2.7	25.0	0.279

Table 2— Dependence of γs on Ci in the Ni-Ni_3B System

T(°C)	γs	Ci (ppm)
1125	3.29×10^{-4}	320
1175	6.24×10^{-4}	257
1225	7.05×10^{-4}	209

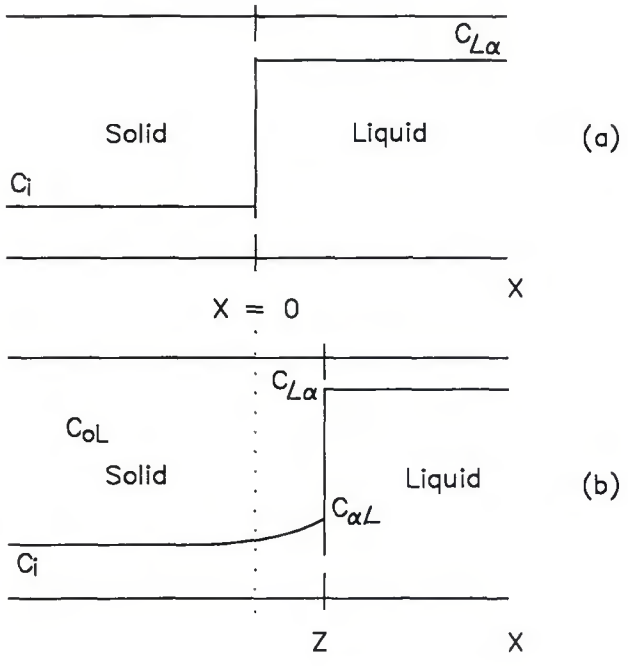

Fig. 12 — Isothermal solidification. A — Initial conditions; B — boundary conditions at t > 0.

will occur in which atoms go from the solid into the liquid phase. Second, the atoms accumulated in the liquid zone next to the solid-liquid interface will migrate into the bulk of the liquid (Ref. 15). The widening of the liquid region or solid-liquid interface displacement will be controlled by the slowest step (reaction at the interface, surface diffusivity, or diffusion in the liquid). At low liquid diffusion rates, the surface reaction may be fast enough to maintain the concentration of solute atoms in the liquid at the interface close to the equilibrium liquid composition. However, if neither step is much faster than the other, both mechanisms may control the process.

The mathematical treatment of this stage was based on the analysis of diffusion in systems with moving boundaries. The assumptions made were: 1) unidimensional diffusion; 2) static liquid, with no convection effect; 3) constant diffusion coefficient; 4) equilibrium at the solid-liquid interface; and 5) semi-infinite media. The initial and boundary conditions are illustrated schematically in Fig. 9. From the mathematical model developed (Ref. 9), the displacement of the solid-liquid interface, Z, during the homogenization and widening of the liquid region stage can be described by Equation (8),

$$Z = \gamma_h \sqrt{4 D_{eff} t_h} \qquad (8)$$

γ_h is a dimensionless parameter, characteristics of the system at a given temperature, that can be determined by numerically solving the following equation:

$$\gamma_h = \frac{C_{oL} - C_{L\alpha}}{C_{L\alpha} - C_{\alpha L}} \cdot \frac{exp(-\gamma_h^2)}{1 + erf(\gamma_h)} \cdot \frac{1}{\sqrt{\pi}} - \frac{C_{o\alpha} - C_i}{C_{L\alpha} - C_{\alpha L}} \cdot \frac{exp(-\gamma_h^2 \phi)}{1 - erf(\gamma_h \sqrt{\phi})} \cdot \frac{1}{\sqrt{\pi \phi}} \qquad (9)$$

D_{eff} is the effective diffusivity and is dependent of the controlling mechanism, that is, diffusion of atoms in the liquid phase or to the reaction at the interface, during the process. In Equation 9, the concentration terms can be determined by using the equilibrium phase diagram. ϕ is the liquid to solid diffusivity ratio, D_L/D_s.

Aside from the initial thickness of the interlayer, the maximum width of the homogenized liquid region, W_m, was found to be a function of the material system.

$$W_m = \frac{2h\rho_o C_o}{\rho_L C_{L\alpha}} \qquad (10)$$

ρ_o and ρ_L are the densities of the solid interlayer and homogenized liquid zone, respectively. From Equation 8, the homogenization time can be determined as:

$$t_h = \frac{Z^2}{4\gamma^2 D_{eff}} \qquad (11)$$

where:

$$Z = \left(\frac{W_m - 2h}{2}\right) = \left[\frac{(2h)}{2}\right]\left[\left(\frac{C_o}{C_{L\alpha}}\right)\left(\frac{\rho_o}{\rho L}\right) - 1\right] \qquad (12)$$

Assuming that ρ_o is equal to ρ_L and rearranging Equations 11 and 12, homogenization time, t_h, can be rewritten as:

$$t_h = \left\{\left(\frac{1}{4\gamma_h\sqrt{D_{eff}}}\right)\left[\left(\frac{C_o}{C_{L\alpha}}\right) - 1\right]\right\}^2 (2h)^2 \qquad (13)$$

The data and numerical solution of γ_h for the Ni-Ni_3B system at 1125°,1175°, and 1225°C are reported in Table 1.

Assuming that boron diffusivity in the liquid phase is the controlling mechanism and that $D_{eff} \approx D_L$, Equation 13 can be rewritten as:

$$t_h = 4.1\times10^{-4}(2h)^2 \text{ at } 1125°C \qquad (14a)$$

$$t_h = 1.3\times10^{-4}(2h)^2 \text{ at } 1175°C \qquad (14b)$$

$$t_h = 1.5\times10^{-4}(2h)^2 \text{ at } 1225°C \qquad (14c)$$

As predicted by the model, the stage of homogenization and widening of the liquid zone required only a few seconds (Fig. 10) and could not be observed experimentally. Figure 10 also shows that increasing the bonding temperature does not always reduce t_h because γ_h is a strong function of the materials system and depends on the characteristics of the corresponding phase diagram.

To confirm the adequacy of the model developed, experimental data for silver-copper diffusion brazing (Ref. 10) were used. From Fig. 7, C_{oL}, $C_{L\alpha}$, and $C_{\alpha L}$ were determined to be 39.5, 29.8, and 12.3 wt-%, respectively, at 820°C (1508°F). The liquid, surface, and lattice diffusivity coefficients (D_L, D_{Surf} and D_s) of copper in silver (Refs. 16–18) are 1.2 X 10^{-5}, 1 X 10^{-6} and 4.6 X 10^{-10} cm^2/s, respectively. Using these data, γ_h was calculated to be 0.235, and therefore,

$$Z = 0.235\sqrt{4 D_{eff} t_h} \qquad (15)$$

where D_{eff} is the effective diffusivity. As mentioned previously, the homogenization process occurs through two sequential steps. Therefore, each of the following expressions for the displacement of the solid-liquid interface may be used depending on which diffusion mechanism is considered to be the controlling one.

$$Z = 126.1\sqrt{t_h} \text{ if } D_{eff} = D_L \qquad (16)$$

$$Z = 36.4\sqrt{t_h} \text{ if } D_{eff} = D_{Surf} \qquad (17)$$

Plotting Equations 16 and 17 with the experimental data, shown in Fig. 11, clearly indicated that interface displacement in the stage of liquid zone homogenization and widening is mainly controlled by surface diffusion of copper in silver. The good correlation shown in Fig. 11 also shows that by considering the relative kinetics of the two sequential steps that may occur, the mathematical model developed is well able to predict the displacement of the solid-liquid

interface during the homogenization of the liquid region.

Isothermal Solidification of the Liquid Zone

When the concentration of the liquid zone reaches $C_{L\alpha}$ the boundary conditions are changed and the solute elements in the liquid region will now diffuse entirely into the base metal. This will lead to a compositional change in the joint and will raise the melting point of the liquid layer. As a result, isothermal solidification occurs and reverses the direction of motion of the interface. And as more diffusion takes place, the liquid layer will eventually disappear, as shown in Fig. 3E. Contrary to the previous stages, isothermal solidification of the liquid region occurs rather slowly and is, thus, the controlling stage of diffusion brazing.

To model isothermal solidification in diffusion brazing as a diffusion problem in systems with moving boundaries, the following conditions were assumed (Ref. 9): 1) unidimensional diffusion; 2) static liquid; 3) constant diffusion coefficient; 4) semi-infinite medium; 5) Equilibrium at the interface; and 6) constant solid-liquid interface area. The initial and boundary conditions are illustrated in Fig. 12.

According to the above assumptions, Ramirez and Liu (Ref. 9) concluded that the displacement of the solid liquid interface, Z, and the time for solidification, t_S, could be determined by the following equations (Ref. 9):

$$Z = \gamma_s \sqrt{4 D_s t_s} \tag{18}$$

$$\gamma_s = \frac{C_{\alpha L} - C_i}{C_{L\alpha} - C_{\alpha L}} \cdot \frac{exp(-\gamma_s^2)}{1 + erf(\gamma_s)} \cdot \frac{1}{\sqrt{\pi}} \tag{19}$$

γ_S is a dimensionless parameter related to the solidification characteristics of the diffusion brazing process and can be calculated by numerically solving Equation 19. D_S is the boron diffusivity in solid nickel.

The progress of solidification was monitored by determining the amount of remaining liquid, W_f, in the braze metal. Figures 13 and 14 illustrate the change in thickness of the remaining liquid film as a function of holding time at several brazing temperatures. While at 1225°C, the nickel-boron-nickel bond solidified after only 30 min, over 100 min were required for the 1125°C specimens to reach complete solidification. The displacement of the liquid-solid interface (indirectly, the width of the remaining liquid), shown in Fig. 14, followed a square root law as a function of time. However, solidification was observed to occur at two different rates. At all temperatures, the liquid-solid interface advanced rapidly during the early part of the process and became significantly slower at longer times. Attempts to understand the basic mechanisms involved in isothermal solidification and to explain the two rate regimes in the controlling stage of diffusion brazing are reported below.

The equilibrium concentrations of the solid ($C_{\alpha L}$) and liquid ($C_{L\alpha}$) at the interface at a given temperature (T) can be expressed as follows:

$$C_{\alpha L} = M_s (T_{MA} - T) \tag{20}$$

$$C_{L\alpha} = M_L (T_{MA} - T) \tag{21}$$

where, M_s and M_L are the slopes of the solidus and liquidus lines, respectively. T_{MA} is the melting temperature of metal A. Using Equations 20 and 21, the fol-

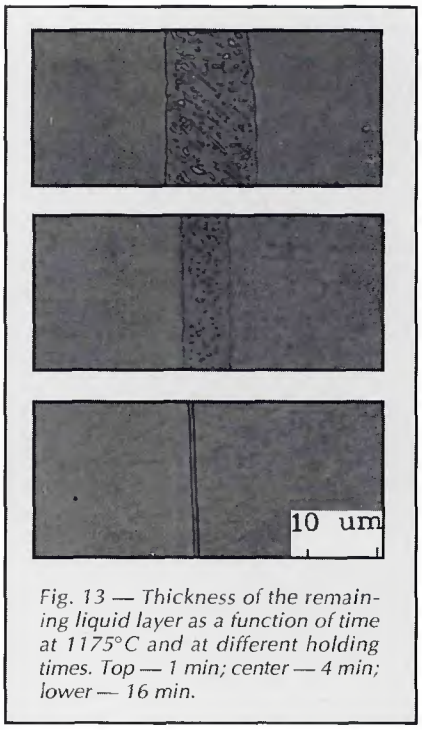

Fig. 13 — Thickness of the remaining liquid layer as a function of time at 1175°C and at different holding times. Top — 1 min; center — 4 min; lower — 16 min.

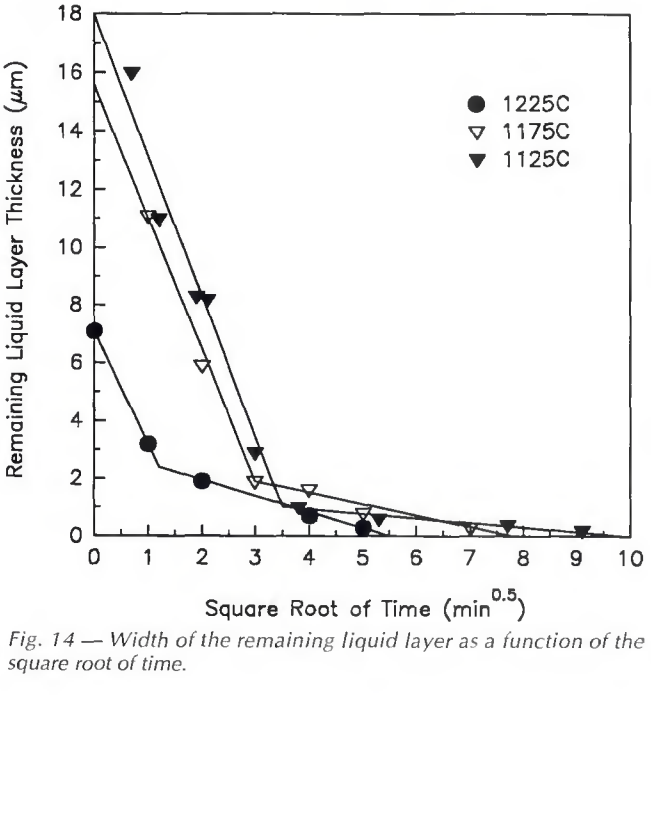

Fig. 14 — Width of the remaining liquid layer as a function of the square root of time.

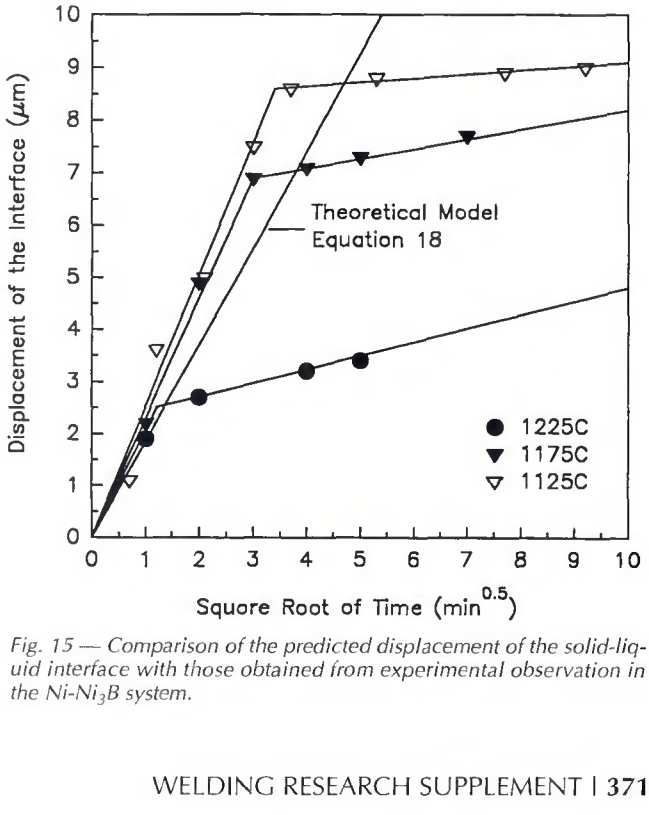

Fig. 15 — Comparison of the predicted displacement of the solid-liquid interface with those obtained from experimental observation in the Ni-Ni_3B system.

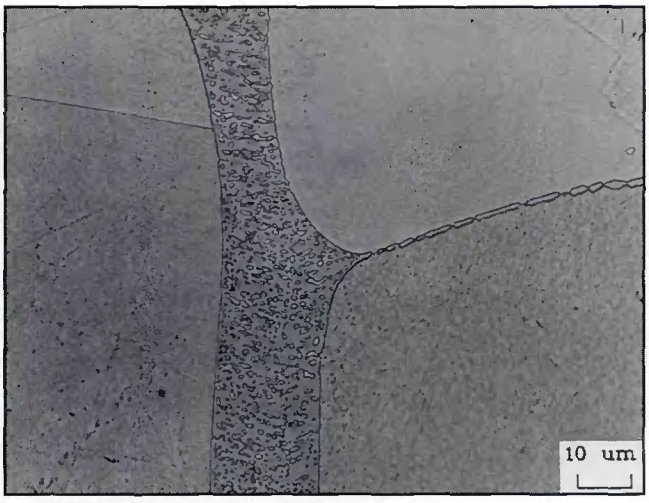

Fig. 16 — Grain boundary penetration observed during diffusion brazing in the Ni-Ni_3B system.

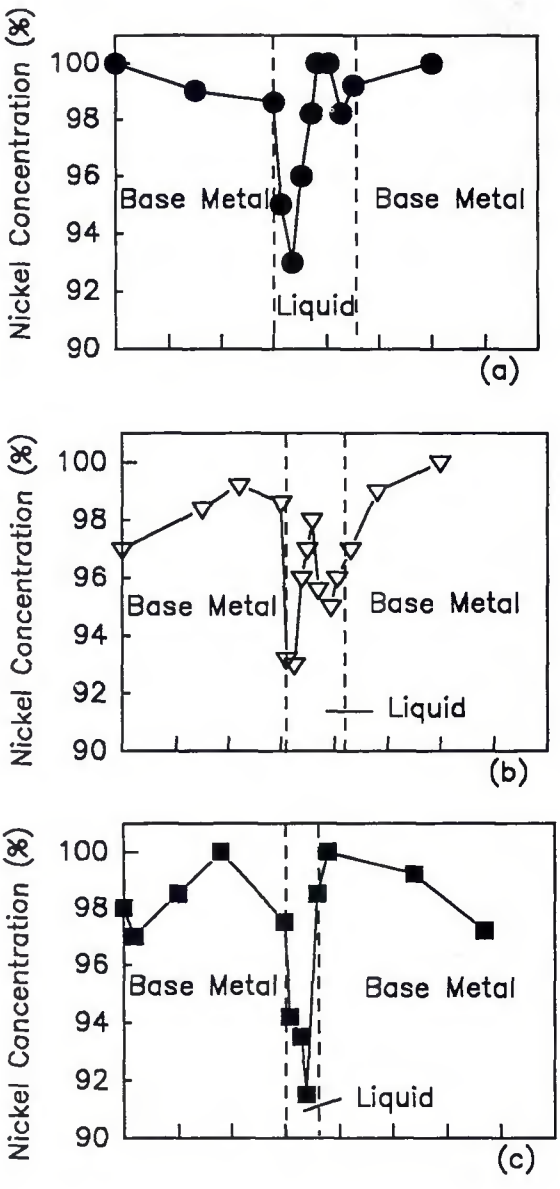

Fig. 17 — Nickel concentration profile across the bond region as determined by electron microprobe analysis. A — 1 min holding time at 1125°C; B — 1 min holding time at 1175°C; C — less than 1 min holding time at 1225°C.

lowing equation can be obtained.

$$\frac{C_{\alpha L} - C_i}{C_{L\alpha} - C_{\alpha L}} = \frac{M_s}{M_L - M_s} - \frac{C_i}{(M_L - M_s)(T_{MA} - T)} \quad (22)$$

The term $M_s/(M_L - M_s)$ is material dependent and usually considered constant for a chosen alloy system. The second term in the right-hand-side member of Equation 22 is temperature dependent. However, since high-purity nickel coupons were used in this work, C_i (initial boron concentration in the base metal) can be assumed to be zero, thus eliminating the temperature dependency. Substituting Equation 22 in 19, γ_s can be rewritten as:

$$\gamma_s = \frac{M_s}{M_L - M_s} \cdot \frac{exp(-\gamma_s^2)}{1 + erf(\gamma_s)} \cdot \frac{1}{\sqrt{\pi}} \quad (23)$$

and for the Ni-Ni_3B system, γ_s was determined to be 6.2×10^{-3}.

Since boron diffusion in nickel is expected to be the controlling mechanism and the diffusion coefficient has been reported (Ref. 19) to be 3.6×10^{-6} cm^2/s, the displacement of the interface can be modeled using Equation 18 as the following expression:

$$Z = 1.82\sqrt{t_s} \quad (24)$$

Comparison of the predicted and experimentally observed solid-liquid interface displacement in Fig. 15 shows that the displacement predicted by the developed model is close to that observed during the initial stage of the solidification process. The small deviation indicates good accuracy of the mathematical model, and that boron diffusivity in solid nickel is indeed responsible for the kinetics of regime 1 in the early part of isothermal solidification.

Liquid Phase Grain Boundary Penetration

The deviation observed during the initial solidification rate regime can be explained as a result of grain boundary penetration of the liquid film as illustrated in Fig. 16. Despite that the modeling of isothermal solidification assumed that the solid-liquid interfacial area remained constant (see assumption 6 in the isothermal solidification section above), penetration of the liquid phase into the base metal along grain boundaries increased considerably the solid-liquid contact area and the solidification. As much as 2500 μm of penetration depth was observed in this research.

Considering the effect of grain boundary penetration, the solute balance at the interface can be expressed as:

$$A_o(C_{L\alpha} - C_{\alpha L})Z = A_r\left(-D_s \frac{dC^s}{dx}\right)_z \quad (25)$$

A_o is the initial base metal interlayer interfacial area and A_r is the total solid-liquid contact area after liquid metal grain boundary penetration occurred. When corrected for the increase in liquid-solid interfacial area, γ_s becomes γ_{sc} with the following expression:

$$\gamma_{sc} = \frac{A_r}{A_o} \cdot \frac{C_{\alpha L} - C_i}{C_{L\alpha} - C_{\alpha L}} \cdot \frac{exp(-\gamma_{sc}^2)}{1 + erf(\gamma_{sc})} \cdot \frac{1}{\sqrt{\pi}} \quad (26)$$

The increase in interfacial area that provided greater boron transfer also resulted in a solidification rate faster than that predicted by the model.

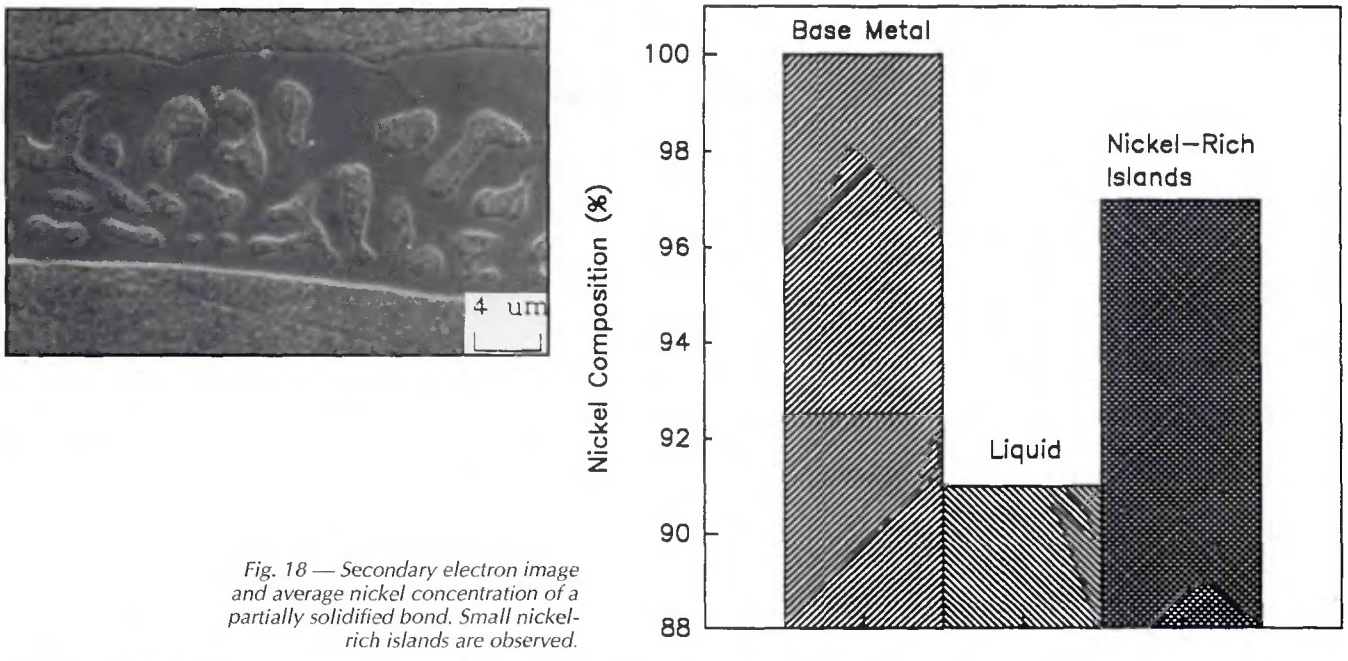

Fig. 18 — Secondary electron image and average nickel concentration of a partially solidified bond. Small nickel-rich islands are observed.

Chemical Composition Changes at the Liquid-Solid Interface

The very slow displacement of the interface during the second regime of isothermal solidification may also be the result of a change in boron concentration in nickel, at or near the liquid-solid interface. This would decrease the chemical composition gradient and the driving force for diffusion of boron into nickel. According to Equations 19 and 22, γ_s, at a given temperature, is dependent of the concentration of boron in nickel, C_i, and can be expressed as:

$$\gamma_s = [\text{constant} - f(C_i, T)] \cdot \frac{exp(-\gamma_s^2)}{1 + erf(\gamma_s)} \cdot \frac{1}{\sqrt{\pi}} \quad (27)$$

Table 2 shows the strong dependence of γ_s on C_i in the range applicable to the Ni-Ni_3B system. Using the best linear fit relation between the interface displacement and square root of time during regime 2 (later on during the solidification process), shown in Fig. 15, γ_s was found to double while C_i was reduced from 320 to 210 ppm between 1125° and 1225°C. Thus, small changes of boron concentration in nickel can produce large changes in the kinetics of the displacement of the interface.

To further investigate this effect, the chemical compositions of the specimens that had experienced solidification in the second regime, particularly in the region next to the solid-liquid interface were determined. Figure 17 shows the concentration distribution of nickel across the bond region. As expected, a gradient of boron composition was observed on the solid side of the solid-liquid interface, which supports the above discussion. Additionally, nickel-rich "precipitate-like" islands were observed to form in the remaining liquid zone as the specimens were cooled from the bonding temperature at the end of the bonding process — Fig. 18. This indicates that element partition was in progress when solidification was interrupted.

Boron Diffusivity Prediction

According to the mathematical model developed, the displacement of the interface, Z, can be expressed as: (see Equation 18)

$$Z = \kappa \sqrt[4]{t} \quad (18a)$$

and,

$$\log Z = \log \kappa + n \log t \quad (28)$$

κ can be determined as the intersection of the best fit line of the experimental results in the first regime of the isothermal solidification stage on a log Z vs. log t plot. Knowing κ, γ_s and γ_{sc}, boron diffusivity in nickel can be determined via the following equations.

$$D_s = \frac{1}{4}\left(\frac{\kappa}{\gamma_s}\right)^2 \quad (29)$$

$$D_{sc} = \frac{1}{4}\left(\frac{\kappa}{\gamma_{sc}}\right)^2 \quad (30)$$

D_{sc} is different from D_s that it takes into consideration the liquid phase grain boundary penetration effect. Table 3 summarizes the findings of n, κ, D_s and D_{sc}. The values of n, between 0.49 and 0.61, showed that regime 1 of solidification indeed followed the square root law and that boron diffusion was the controlling mechanism. D_s varied from 1.8×10^{-6} to 5.2×10^{-6} cm²/s. D_{sc} was found to vary from 1.0×10^{-6} to 4.5×10^{-6} cm²/s, in close agreement with the diffusion coefficients reported in the literature (Ref. 19).

In addition to diffusivity, the activation energy of boron diffusion in nickel

Table 3 — Exponenial Coefficient (n), log κ Values (from the Logarithmic Relation between Z and t), D_s, and D_{sc} Values

Regime	T(°C)	n	log κ	D_s (cm²/s)	D_{sc} (cm²/s)
1	1125	0.61	−4.775	1.84×10^{-6}	1.01×10^{-6}
	1175	0.51	−4.563	4.88×10^{-6}	2.97×10^{-6}
	1225	0.49	−4.572	5.20×10^{-6}	4.48×10^{-6}

Table 4 — Diffusivity of Carbon, Boron and Beryllium in Nickel[a]

Solute	D Equation	T(°C)
C	$0.37\exp\left(\frac{-35700}{RT}\right)$	860–1100
B	$3.27\exp\left(\frac{-39700}{RT}\right)$	1125–1225
Be	$0.02\exp\left(\frac{-46200}{RT}\right)$	1020–1400

(a) Refs. 20, 21.

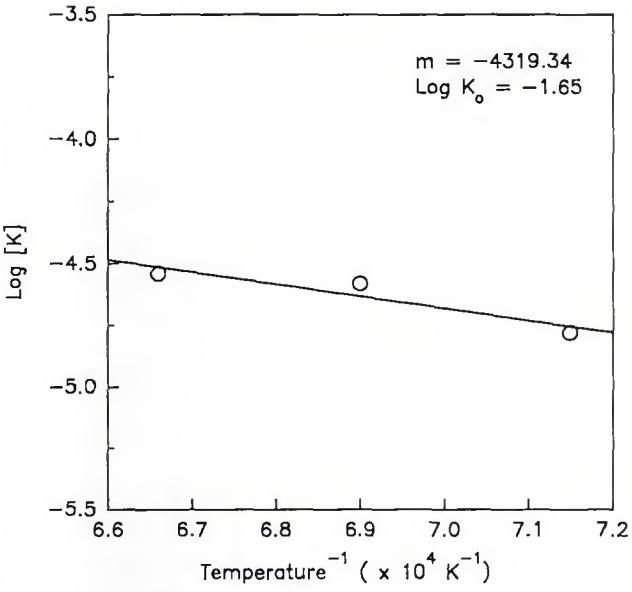

Fig. 19 — Solidification of the liquid region in the Ni-Ni_3B system: Log K as a function of the inverse temperature (1/T).

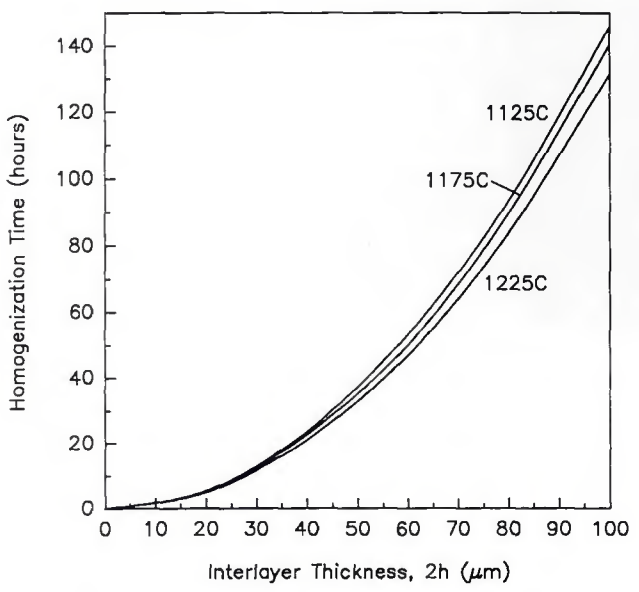

Fig. 20 — Homogenization time as a function of interlayer thickness. The final concentration of boron at the centerline of the bond was assumed to be 100 ppm.

was also determined in the present work. κ from Equation 18a can be rewritten as:

$$\kappa = \gamma_s\sqrt{4D_s} = \gamma_s\sqrt{4D_o}\ exp\left(\frac{-Q}{2RT}\right) \quad (31)$$

where D_o is the frequency factor in cm^2/s and Q is the activation energy of boron diffusion in Cal/mol. R is the universal gas constant and T is the processing temperature. The logarithmic form of Equation 31 is:

$$\log\kappa = \log\kappa_o - m\frac{1}{T} \quad (32)$$

where,

$$\kappa_o = \gamma_s\sqrt{4D_o} \quad (33)$$

and

$$m = \frac{Q}{2*2.3R} \quad (34)$$

D_o and Q were evaluated by plotting log κ as a function of 1/T in the form of an Arrhenius plot (Fig. 19) and had values of 3.27 cm^2/s and 39,700 Cal/mol, respectively. Thus,

$$D = 3.27\,exp\left(\frac{-39,700}{RT}\right) \quad (35)$$

This result is different from that reported in the literature (Ref. 19).

$$D = 2.3\times10^{-3}\,exp\left(-\frac{19,000}{RT}\right) \quad (36)$$

Disagreement between the two results is possibly because of experimental errors in a relatively narrow range of diffusion brazing temperature, for example, 1140° to 1180°C (2084° and 2156°F) (Ref. 19). The temperature range of 1125° to 1225°C investigated in the present work was considerably larger than those found in the literature.

The activation energy determined seems to be reasonable when compared with the activation energy reported for carbon (Ref. 20) and beryllium (Ref. 21) in nickel, Table 4. The activation energy for atom diffusion in a given matrix increases as the atomic radius of the diffusing element increases. The atomic radius of carbon, boron, and beryllium increase in that order and thus, an increase is expected for the activation energy.

Homogenization of the Solidified Bond Region

Holding the solidified joint at a high temperature will lead to extensive diffusion of the elements in the braze region into the base metal, which ensures a uniform distribution of the alloying elements throughout the brazement. Thus, the final composition and microstructure of the brazed joint will closely resemble that of the base metal.

According to the mathematical model developed, the time necessary to reduce the concentration of the solute at the centerline of the joint, from C_o to a required level C_r, is given by the following equation.

$$t = \left(\frac{1}{\kappa_2^2} - \frac{1}{\kappa_1^2}\right)\frac{(2h)^2}{16D_s} \quad (37)$$

where,

$$\frac{C_{at}}{C_o} = erf(\kappa_1) \quad (38)$$

and

$$\frac{C_r}{C_o} = erf(\kappa_2) \quad (39)$$

C_r is the desired composition after homogenization. Figure 20 gives the time required to reduce the boron concentration at the centerline of a Ni-Ni_3B-Ni diffusion brazed joint to 100 ppm as a function of the initial thickness of the interlayer.

Conclusions

Based on the modeling and experimental results obtained, the following conclusions are made:

1) Pack cementation is efficient in providing a thin and uniform layer of Ni_3B on nickel for diffusion brazing.

2) The mathematical model proposed describes well the kinetics of the four stages of diffusion brazing, as a function of processing temperature, interlayer thickness and composition, and the phase diagram of the Ni-Ni_3B system.

3) The first two stages, dissolution and melting of the Ni_3B interlayer, and homogenization of the liquid zone are extremely fast, requiring seconds or less for completion.

4) Isothermal solidification of a Ni-Ni_3B-Ni diffusion bond occurs slowly with boron diffusion in solid nickel as the controlling mechanism.

5) The kinetics of isothermal solidification can be divided into two regimes: a faster initial regime and a sluggish final regime. Liquid phase penetration along the grain boundaries provides an increased solid-liquid interfacial area for

boron transfer, and it is responsible for the faster kinetics regime.

6) The variation of boron concentration at the interface during solidification changes the kinetics of the process and is responsible for the slower second regime.

7) The activation energy for boron diffusion in nickel, estimated to be 39.7 kCal/mol, compared well with diffusivities of carbon and beryllium in nickel.

Acknowledgement

Author, J. E. Ramirez, gratefully acknowledges the financial support of the Instituto Colombiano del Petroleo.

References

1. Peaslee, R. L., and Boam, W. M. 1952. Design properties of brazed joints for high temperature applications. *Welding Journal* 31(8):651–662.

2. Paulonis, D. F., Duvall, D. S., and Owczarski, W. A.. 1972. U.S. Patent 3,678,570.

3. Sekerka, R. F. 1980. On the modeling of diffusion bonding. *Proc. on Physical Metallurgy*, p. 1, TMS-AIME, St. Louis, Mo.

4. Lesoult, G. 1976. Modeling of the diffusion bonding process I. Report of Center for the Joining of Materials, Carnegie-Mellon University,Pittsburgh, Pa.

5. Ed. V. I. Matkovich. 1977. *Boron and Refractory Borides*, Springer-Verlag.

6. Moffat, W. G. 1984. *The Handbook of Binary Phase Diagram*, Vol. 1, General Electric Co., Schennectady, N.Y.

7. Schobel, J. D., and Stadelmair, H. Z. 1965. Das zweistoffsystem nickel-boron, *Z. Metallkunde*, 56, pp. 856–859.

8. Gasele, V., and Tu, K. N. 1982. Growth kinetics of planar binary diffusion couples. *Journal of Applied Physics*, 53(4):3252–3260.

9. Ramirez, J. E. 1989. Modeling of diffusion bonding in nickel-boron system. M.S. thesis T-3751, Colorado School of Mines, Golden, Colo.

10. Tuah-Poku I., Dollars, M., and Massalski, T. B.. 1988. A study of the diffusion bonding process applied to a Ag/Cu/Ag sandwich joint. *Metallurgical Transactions - A*, V. 19A, pp. 675–686.

11. Liu, S., Olson, D. L., Martins, G. P., and Edwards, G. R. 1990. The use of coating and interlayer technology in brazing. *Welding Journal* 70(8):207-s to 215-s.

12. Eds. J. M. Poate and J. M. Mayer. 1978. Ag-Cu phase diagram. *Thin Films-Interdiffusion and Reactions*, John Wiley, N.Y.

13. Podstrigach, Y. S., and Shevchuk, P. R. 1973. Effect of thin coatings and intermediate layers on diffusion processes and stresses in solids. *Protective Coatings on Metals*. Vol. 5, pp. 247–252.

14. Semenov, A. P., Pozdnyakov,V. U., and Waposhina, L. B. 1972. Contact eutectic melting as a method of producing surface coatings. *Protective Coatings on Metals*. Vol. 4, pp. 216–220.

15. Lammel, J. M., and Chalmers, B. 1959. The isothermal transfer from solid to liquid in metal systems. *Trans. of the Metallurgical Society of AIME*, pp. 499–508.

16. Yamarura, T., and Ejima, T. 1973. Japan Institute of Metals, Vol. 37, pp. 901–907.

17. Butrynowicz, D. B., Manning, J. R., and Read, M. E. 1974. Diffusion in copper and copper alloys.,*J Phys. Chem.*, Ref. Data, Vol. 3, pp. 327–602.

18. Hall, M. G., and Haworth, C. W. 1969. The diffusion of copper in silver(rich)-copper alloys. Trans. AIME, Vol. 245, pp. 2476–2479.

19. Liping, D., Fengzhi, Y., and Yugin, G. 1982. The diffusion honding of superalloys K18 and the diffusion behavior of element boron. *Hanjie Xuebao*. 3(3):84–98.

20. Smith, R. P. 1966. The diffusion of carbon in gamma iron-nickel alloys.. Trans. AIME. Vol. 236, pp.1224–1227.

21. Grigorev, G. V., and Pavlino, L. V. 1968. Diffusion of Be in Fe and Ni. *Fiz. Metal. Metalloved*, 25(5):836–839.

American Welding Society Conference Planner

October 19-21, 1992 - Columbus, OH

Eighth North American Welding Research Conference: Recent Developments in the Joining of Stainless Steels and High Alloys

This conference is directed to the producers and users of stainless steels and high-performance Ni-based and Co-based alloys. Special topics will include austenitic stainless steels, duplex stainless steels, and high-performance alloys.

November 3-6, 1992 - Orlando, FL

Int'l Conference on Computerization of Welding Information IV

Topics will highlight data formats and searchable standards, weld sensing for real time control, quality and non-destructive examination, welding engineering applications, weld controllers and control systems, and databases and welding procedures. A hands-on computer exhibition will also be featured.

November 9-11, 1992 - Pittsburgh, PA

ISO 9000 - A Quality System Workshop

This intensive workshop, designed for fabricators who use welding procedures, will compare the new European Community standards for welding procedures and welder performance qualifications with existing U.S. welding design and fabrication standards. Registration is limited to 20.

February 3-5, 1993 - San Francisco, CA

Golden Gate Materials Technology Conference

Topics will include advanced welding methods and equipment, structural welding high-strength and conventional steels, advancements in metals and composites, modern approaches to corrosion prevention, improvements in nondestructive inspection technologies and strategies, new approaches to materials characterization and process modeling, and improvements in productivity, reliability and profitability. An exhibition will be featured.

For further information and registration details, call or write AWS Conferences, 550 N.W. LeJeune Road, Miami, Florida 33126, 800-443-9353, Ext. 278 .